DETAILED MODELLING OF CHARGING BEHAVIOUR OF SMART SOLAR TANKS

Fan, Jianhua; Andersen, Elsa; Furbo, Simon; Perers, Bengt

Published in:
Proceedings of EuroSun 2010

Publication date:
2010

Document Version
Publisher's PDF, also known as Version of record

DETAILED MODELLING OF CHARGING BEHAVIOUR OF SMART SOLAR TANKS

Jianhua Fan*, Elsa Andersen, Simon Furbo and Bengt Perers

Department of Civil Engineering, Technical University of Denmark,

Brovej, building 118, DK-2800 Kgs. Lyngby., Denmark.

* Corresponding Author, jif@byg.dtu.dk.

Abstract

The charging behaviour of smart solar tanks for solar combisystems for one-family houses is investigated with detailed Computational Fluid Dynamics (CFD) modelling and Particle Image Velocimetry (PIV) measurements. The smart solar tank can be charged with a variable auxiliary volume fitted to the expected future energy demand. Therefore the heat loss from the tank is decreased and the thermal performance of the solar heating system is increased compared to a traditional system with a fixed auxiliary volume. The solar tank can be charged either by an electric heating element situated in the tank or by an electric heating element in a side-arm mounted on the side of the tank. Detailed CFD models of the smart tanks are built with different mesh densities in the tank and in the side-arm. The thermal conditions of the tank during charging are calculated with the CFD models. The fluid flow and temperature calculations are compared to PIV (Particle Image Velocimetry) measurements of fluid flows and temperature measurements. The aim is to elucidate the temperature distribution and thermal stratification of the tank during charging. It is elucidated how the calculated temperatures in the tank are influenced by the mesh densities, the distribution of computational cells, the physical model and time steps used in the simulations. The findings of the investigations will be used as guidance for creation of CFD models for optimal design of smart solar tanks.

1. Introduction

The two most powerful renewable energy sources are solar and wind energy. It is expected that an increasing part of the electricity consumption in the future will be covered by wind farms. This will result in an increased number of windy periods with a surplus of electricity and thereby a low electricity price. A concept where individual solar heating systems are optimised for making use of electricity produced by wind turbines in these periods can facilitate the introduction of wind energy on a large scale into the energy system and thereby contribute to increasing the part of the energy consumption covered by renewable energy sources.

An ongoing research project will elucidate how best to design an individual heating unit for one-family houses based on smart solar tanks [1]. The project will elucidate how suitable the heating unit is for the home owner and for our future energy system. Different designs of the heating unit and the control system will be investigated.

The heat of the energy system will be produced by a solar heating system and by electrical heating element(s). The electrical heating element(s) will, if possible, only be in operation in periods where the

solar heating system cannot cover the heat demand of the house 100% and where the electricity price is low, for instance due to high energy production from wind farms or due to a low electricity consumption. The energy system will need a smart heat storage with a variable water volume heated by low cost electricity and an advanced control system for the electric heating element(s)/heat pump based on prognosis for electricity costs, heat demand and solar heat production and a control system based on weather forecasts. The tank can be charged with a variable volume by internal heating elements installed at different levels in the tank or by a side-arm with a heating element.

This paper focuses on detailed modelling of the auxiliary charging, by means of electric heating element(s), of such a smart solar tank for solar combisystems for a one-family house. The focus of the study on the tank with a heating element in the tank is the flow field around the heating element during charging and how the fluid flow influences thermal stratification at the top of the tank. For the tank with a side-arm, the tank is charged by thermosyphon induced circulation through the side-arm. The charging of the tank is influenced by the power of the electric heating element, the position of the electric heating element and the design of the side-arm, for example, diameter of the side-arm pipe and position of the side-arm connection to the tank, etc. The focus of the study on the tank with a side-arm is to investigate how the design of the side-arm and the operating conditions influence charging behaviour of the tank. The ultimate aim of the study is to validate CFD models of the smart solar tanks and to give recommendations for creation of the CFD models for optimization of smart solar tanks.

2. Experimental and Theoretical Investigations

The auxiliary charging behaviour of a tank is investigated theoretically by CFD calculations and experimentally by PIV measurements. To facilitate the PIV measurements, a square glass tank is built with a cross section of 400 mm x 400 mm and a height of 900 mm, see Fig. 1. The uninsulated tank is made of 12 mm glass with a thermal conductivity of 0.81 W/mK.

Fig. 1. The PIV test facility of the smart solar tank with one heating element and a side-arm.

The tank is designed in such a way that it can be charged either by an electric heating element situated in the tank or by an electric heat element in a side-arm mounted on the side of the tank. The internal electric heating element is situated in the tank at a height of 450 mm from the bottom of the tank. One end of the side-arm is mounted on the side of the tank with a distance of 800 mm from the tank bottom while the other end of the side-arm is mounted on the centre of the tank bottom. The side-arm has a built in electric heating element which gives a variable charging power from 1 kW to 3 kW. PIV equipment from Dantec Dynamics is used to determine the fluid flow in the tank, especially in the

upper part of the tank where water is heated either by the internal heating element or by the side-arm. Thermal stratification in the tank is measured at different levels by temperature sensors located in one corner of the tank. The accuracy of the temperature measurement is estimated to be 0.5 K. The measured temperatures are compared to temperatures calculated by the CFD models.

The CFD model of the tank with an internal electric heating element is shown in Fig. 2. The mesh on the vertical cut-plane of the tank is shown in Fig. 2 (a). A. In order to better resolve the heat transfer and fluid flow in the region adjacent to the electric heating element and in the region adjacent to the tank wall, a boundary layer mesh is applied so that there is a fine and dense mesh in these regions, see Fig. 2(a) and 2(b). The 3D tank model includes the glass tank wall as a solid region and the hot water volume of the tank as a fluid region. The charging of the electric heating element is modelled as heat flux from the surface of the heating element. The power of the heating element is 500 W which corresponds to a heat flux of 30041 W/m^2. A size function is used to assign denser mesh around the electric heating element where a high temperature gradient is expected. A non-slip wall condition is used for all wall surfaces except the top of the tank where there is free water surface. A zero shear stress wall condition is used for the top inner surface of the tank. The heat loss from the tank is calculated by surface heat transfer coefficients of the tank wall and the temperature differences between the glass tank and the ambient air. The surface heat transfer coefficients of the top, the side and the bottom of the tank are 10 W/m^2K, 7.69 W/m^2K and 5.88 W/m^2K respectively. The Ambient air temperature is constantly 20°C.

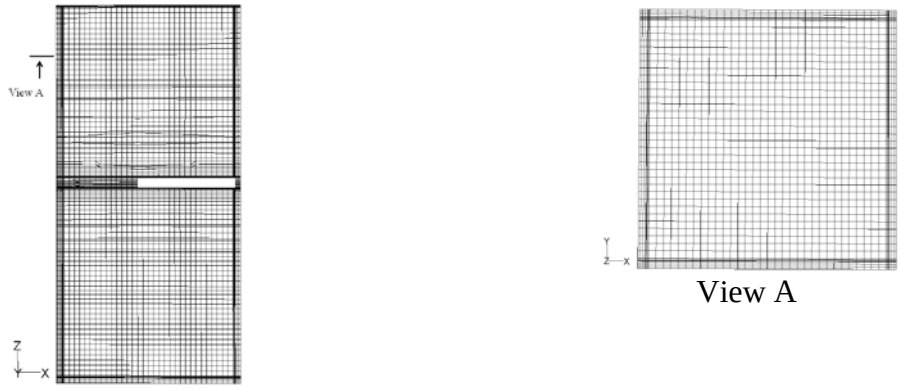

(a). Vertical middle plane of the model (b). Cross section of the model

Fig. 2. CFD model of the tank with an internal electric heating element

The CFD model of the tank charged with a side-arm is shown in Fig. 3. The vertical cut-plane through the middle of the tank is given in Fig. 3(a). A boundary layer mesh is applied to the surface of the heating element, the inner surface of the side-arm and the inner surface of the tank where high temperatures and/or velocity gradients are expected, see Fig. 3(b). The tank is charged by thermosyphon induced circulation through the side-arm. Modelling of fluid flow and heat transfer in the side-arm is therefore critical. A denser mesh is applied to the side-arm while a coarse mesh is applied to the tank body, see Fig. 3(c). An interface is used to combine the non-conformal mesh of the upper half and the bottom half of the tank. The side-arm consists of two sections of copper pipes of 28 mm outer diameter and one section steel pipe with an outer diameter of 66 mm with a built in electric heating element. The 3D tank model includes the glass wall of the tank and the copper/steel pipe walls of the side-arm as solid regions, and the hot water volume in the tank and in the side-arm as fluid regions. The charging of the electric heating element is modelled as a heat flux from the surface of the

heating element. The power of the heating element is 3kW which corresponds to a heat flux of 97607 W/m^2. A non-slip wall condition is used for all wall surfaces except the top surface of the tank where a zero shear stress wall condition is applied. Heat loss from the tank is modelled the same way as for the tank with an internal heating element. The side-arm is insulated with a heat transfer coefficient of 2.4 W/m^2K between the pipe outer surface and the ambient air.

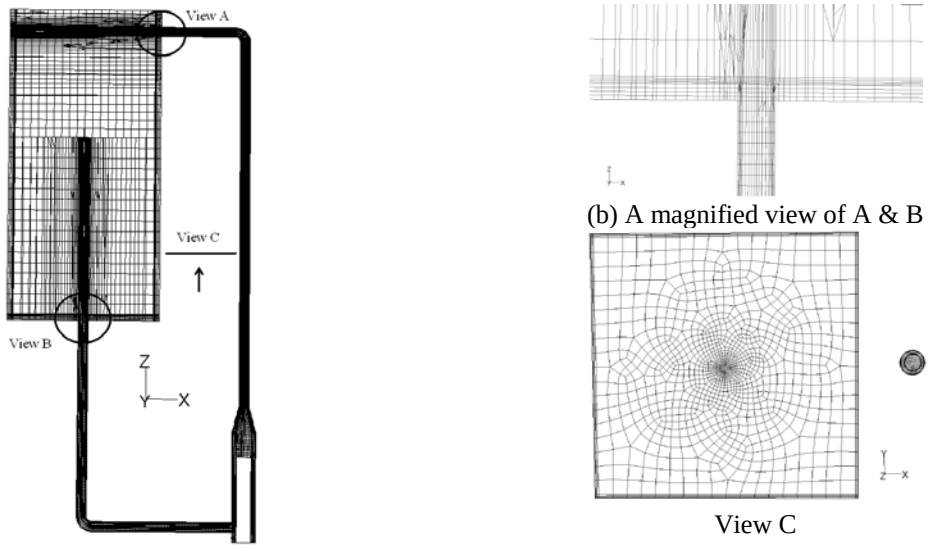

(b) A magnified view of A & B

(a) Middle plane of the model

(c) Cross section of the model

Fig. 3. CFD model of the tank with electric heating element built in a side-arm

Water is used as the heat storage media. Properties of water and their dependences on temperature are shown as follows:

Dynamic viscosity, [kg/(ms)] $$\mu = 0.0007 * (\frac{T}{315})^{-5.5} \quad (1)$$

Thermal conductivity, [W/(mK)] $$\lambda = 0.375 + 8.84 \times 10^{-4} * T \quad (2)$$

where T is fluid temperature, [K].

The tank wall material, glass, has a thermal conductivity of 0.81 W/mK, while copper and steel has a thermal conductivity of 388 and 60 W/mK, respectively.

The Reynold number of the flow in the side-arm is estimated to be between 3000-4000 which indicates a flow in the transitional region. The flow around the heating element is most likely turbulent due to the high power of the electric heating element. A RNG k-ε turbulence model is therefore used to model the flow.

Transient CFD calculations are carried out with buoyancy driven force modelled by Boussinesq approximation [2]. The PRESTO and second order upwind method is used for the discretization of the pressure and the momentum/energy equations respectively [2]. The SIMPLE algorithm is used to treat the pressure-velocity coupling. The transient simulations start with a tank with a uniform temperature of 20.3˚C and a zero velocity field in the tank. The calculation is considered convergent if the scaled residual for the continuity equation, the momentum equations and the energy equation are less than 10^{-3}, 10^{-3} and 10^{-6}, respectively. The simulation runs with a time step between 1-10 s and a duration of 1

hour. One simulation with a time step size of 3 s takes approx. 12-52 hours for a duo core processor computer with 2 X 3 GHz CPU frequency and 4G memory.

3. Results and Discussion

3.1. Influence of grid density and time step size

Investigations are carried out to determine the optimal time step and grid density. Time intervals in the range of 1-10 s are investigated. The mesh scheme of the tank with an internal electric heating element is listed in Table 1. The minimum mesh interval size is applied to the region adjacent to the surface of the electric heating element. The mesh interval size increases with a ratio of 1.1 further away from the heating element until it reaches the maximum mesh interval size. In the rest of the tank, the maximum mesh interval size is used. A 4-row boundary layer mesh is assigned to the surface of the tank wall and the surface of the heating element. The height of the first row of mesh is listed in Table 1 for different mesh schemes. The height of the boundary layer mesh increases with a ratio of 1.2 away from the wall surface. Four mesh schemes are investigated with mesh interval sizes between 0.001 and 0.03 m.

The mesh scheme of the tank with a side-arm is listed in Table 2. The mesh size varies between 0.004 m and 0.008 m in the side-arm, while it varies between 0.012 m and 0.03 m in the tank body. Four-row boundary layer mesh is attached to all wall surfaces of the tank and of the side-arm. The first row height of the boundary layer mesh is 0.001 m for the tank wall surfaces while it is either 0.0002 m or 0.0005 m for the wall surfaces of the side-arm.

Table 1. Mesh schemes of the tank with an internal electric heating element.

	Number of cells	**Mesh interval size, [m] Min./Max.**	**Boundary layer mesh, the first row height, [m]**
Grid 1	37,525	0.002/0.03	0.001
Grid 2	193,522	0.002/0.012	0.001
Grid 3	495,936	0.001/0.008	0.001
Grid 4	1,192,380	0.001/0.006	0.0005

Table 2. Mesh schemes of the tank with a side-arm with built in electric heating elements.

	Number of cells	**Mesh interval size, [m]**		**Boundary layer mesh, the first row height, [m]**	
		Tank	**Side-arm**	**Tank**	**Side-arm**
Grid 1	189,698	0.03	0.008	0.001	0.0005
Grid 2	263,768	0.03	0.006	0.001	0.0005
Grid 3	407,314	0.012	0.006	0.001	0.0005
Grid 4	761,465	0.012	0.004	0.001	0.0002

CFD predicted thermal stratification in the tank with a side-arm is shown in Fig. 4 and 5. The influence of mesh density on prediction of temperatures in the tank is shown in Fig. 4. At 10 min after the start of the charge, the difference between the temperatures predicted by Grid 2, Grid 3 and Grid 4 is maximum 0.7 K, while the difference between Grid 1 and Grid 4 is up to 2.7 K. The influence of mesh density on predicted temperature becomes less dominant as the test goes on. The difference of temperature predictions between Grid 1 and Grid 4 is decreased to maximum 2.0 K at 60 min after the start. It can be concluded that the mesh scheme Grid 2 is appropriate for modelling the tank with a side-arm. The influence of mesh density and time step size on prediction of temperature distribution in the tank with an internal heating element is investigated as well. The results show that the mesh

scheme Grid 2 is appropriate for modelling the tank with an internal heating element. Fig. 5 shows the influence of a time step size on temperature predictions in the tank. If a time step size between 1 s and 3 s is used, the difference of temperature prediction is within 0.5 K. With an increase of the time step size to 5 s and 10 s, the variation of temperature calculation increases up to 1.7 K and 5 K. It can be concluded that a model with a time step size between 1 s and 3 s can predict temperatures for most of the tank within an uncertainty of 0.5 K. Due to the dramatic increase of computation time with a decrease of the time step size, a time step of 3 s is used for later calculations.

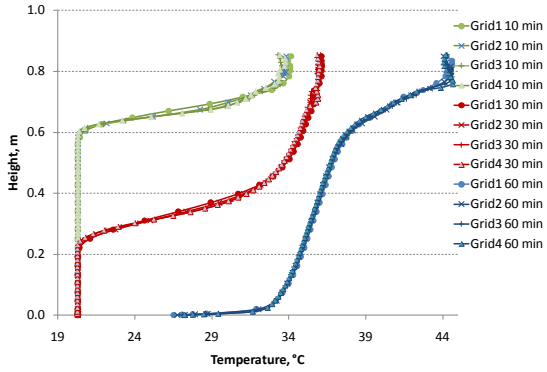

Fig. 4. Influence of mesh density on prediction of thermal stratification in the tank with a side-arm

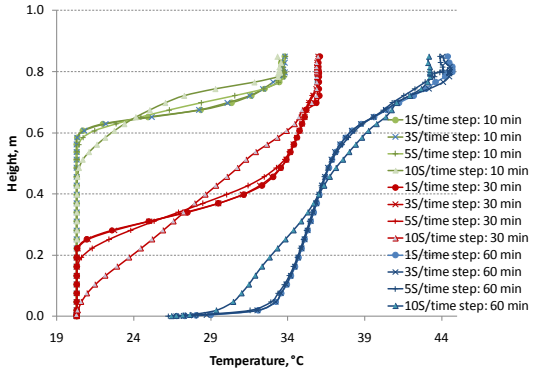

Fig. 5. Influence of time step size on prediction of thermal stratification in the tank with a side-arm

3.2. Thermal stratification in the tanks

The CFD model with Grid 2 is used with a time step size of 3 s for the calculation of heat transfer and fluid flow in the tanks. The convective heat loss and thermal radiation heat loss from tank surfaces are now considered. The surface convective heat transfer coefficient for the side, the top and the bottom of the tank are respectively $1.49(T-T_a)^{0.33}$, $1.55(T-T_a)^{0.33}$ and $0.68\left(\frac{T-T_a}{l}\right)^{0.25}$ where T is the surface temperature of the tank; T_a is the ambient air temperature of the room; l is the dimension of the tank in m. The thermal radiation heat transfer coefficient is defined as:

$$\frac{\sigma(T+T_a)\left(T^2+{T_a}^2\right)}{\frac{1}{\varepsilon_T}+\frac{1}{\varepsilon_a}-1}$$

where σ is Stefan–Boltzmann constant, 5.67E10-8 W/m^{2}K^4. ε_T is the emittance of the tank surface, 0.8; ε_a is the effective emittance of the surrounding surfaces which is assumed to be 0.8. The ambient air temperature increases as the room is gradually heated up by the heat loss from the tank. A temperature of 20.3°C is used from the start till 30 min after the start, while 22.3°C is used for the rest of the test.

CFD calculated temperatures are compared to the measured temperatures. Fig. 6 shows CFD calculated and measured temperatures at different levels in one corner of the tank. The electric heating element with a power of 460 W is installed at a height of 0.45 m. It can be seen in Fig. 6 that after the start of the charging, the water above the level of the element is gradually heated up to almost uniform temperature. There is almost no thermal stratification at the upper part of the tank, which means that the uprising flow from the heating element induced by buoyancy driven force creates mixing in the upper part of the tank. The water at the bottom part of the tank is not heated, indicating that the uprising flow from the element is not large enough to disturb water in the bottom part of the tank. At

58 min after the start, the water temperature in the upper part of the tank increases to 25.0°C, while the water temperature at the bottom part is only slightly higher than 20°C due to heat conduction of water and the glass tank wall. The CFD model predicts well temperatures in the tank with a difference of maximum 0.3 K, especially in the upper part of the tank. The difference is most likely due to the incorrect input of surface heat transfer coefficients and ambient air temperature in the CFD model.

Fig. 7 shows thermal stratification in the tank charged by a side-arm with a power of 3kW. One end of the side-arm is mounted on the side of the tank at a height of 0.8 m, while the other end of the side-arm is mounted on the centre of the tank bottom. The water in the side-arm is heated to a higher temperature than the water in the tank, which generates buoyancy driven flow in the side-arm. The uprising flow in the side-arm creates circulation of water between the side-arm and the tank. Temperatures at different heights in one corner of the tank is measured and compared to CFD calculations in Fig. 7. The CFD model predicts well thermal stratification in the tank at 10 min and 30 min after the start of the charging. But it underestimates temperatures in the tank at 60 min after the start, especially at the height of 0.4 m to 0.7 m. The reason could be an overestimated heat loss from the tank.

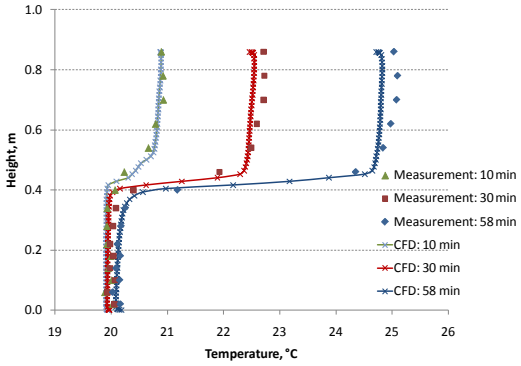

Fig. 6. Thermal stratification in the tank with an internal heating element

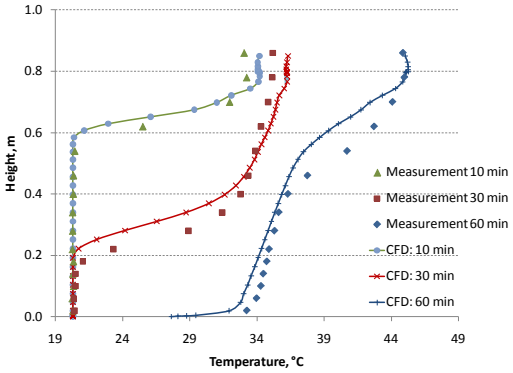

Fig. 7. Thermal stratification in the tank with a side-arm

The heat transfer and fluid flow in the side-arm has a significant influence on the charging behaviour of the tank. Fig. 8 shows the temperature of the fluid entering into the side-arm. There is a good agreement between measured and calculated temperatures. Fig. 9 shows the temperature of the fluid entering into the tank. CFD predicts a flux of hot water entering into the tank 48 s after the electric heating element is turned on, while it is undetected during the measurement. That could be explained by the fact that the temperature sensor is installed on the outer surface of the copper pipe which makes it difficult to respond to the fast temperature changes of the water in the pipe. There is a difference of maximum 3 K between the measurements and the CFD predictions, which is probably due to a slight underestimation of circulation flow in the side-arm. The calculations show that the volume flow rate through the side-arm varies between 2.6-3.4 l/min during the test.

3.3. Fluid flow in the tank with a side-arm

Fig. 10 shows PIV measured fluid flow on the middle plane of the upper part of the tank 5 min after the start. The fluid entering into the tank from the side-arm forms a jet flow. The jet flow reaches the other side of the tank and turns back, forming a circulation. Because of the jet flow and the induced circulation, the tank above the side-arm inlet is mixed. That can be verified by the uniform temperature in the tank above 0.78 m, see Fig. 7. Fig. 11 shows CFD predicted flow field on the middle plane of

the upper part of the tank 5 min after the start. The CFD model predicts successfully the flow pattern, although the velocity magnitude of the flow is overestimated. Another reason for the lower fluid flow in the PIV measurement could be the uncertainty of PIV measurement which is influenced by the specification of duration between pulses and the method used for analysis of the particle image. These factors should be further investigated in future work.

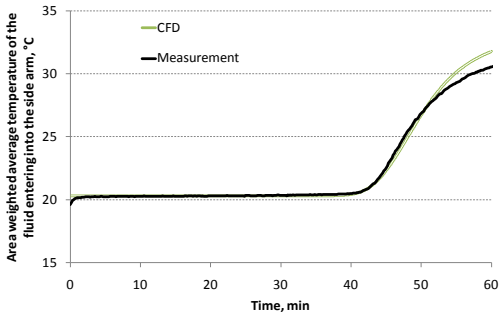

Fig. 8. Temperature of the fluid entering into the side-arm

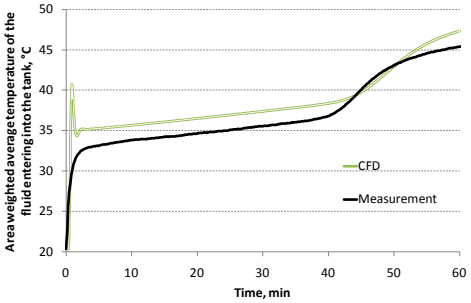

Fig. 9. Temperature of the fluid entering into the tank

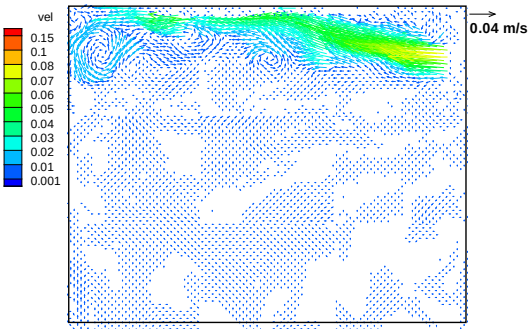

Fig.10. PIV measured flow field on the middle plane of the tank 5 min after the start

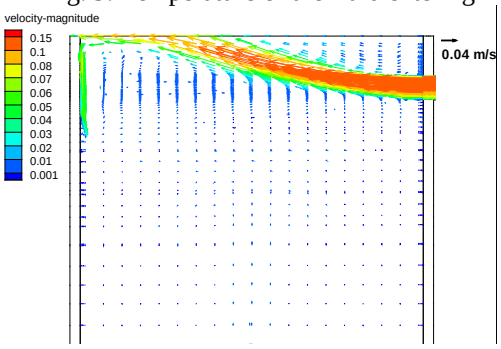

Fig.11. CFD predicted flow field on the middle plane of the tank 5 min after the start

5. Conclusions

The charging behaviour of two smart solar tanks is investigated with detailed CFD modelling and PIV measurements. The solar tank can be charged either by an electric heating element situated in the tank or by an electric heating element in a side-arm mounted on the side of the tank. The results show that a mesh interval size of 0.03 m and 0.006 m is sufficient for the tank and the side-arm, respectively. The most appropriate time step size is 3 s. The fluid flow and temperature calculations are compared to PIV measurements and temperature measurements. The CFD model predicts well thermal stratifications in the tank, but gives underestimated temperatures due to incorrect heat loss of the tank which should be further investigated. The CFD model predicts successfully the flow pattern in the tank, although the velocity magnitude of the flow is higher than the PIV measurements.

References

[1] B. Perers, S. Furbo, E. Andersen, J. Fan. Solar/electric heating system for the future energy system. ISES Solar World 2009 Congress Proceedings. Johannesburg 2009.

[2] Fluent Inc., 2006. “Fluent release 6.3”, 10 Cavendish Court, Lebanon, NH 03766-1442 USA.

[3] O. B. Stampe, Glent Ventilation, Glent & CO A/S, 1977.